FUNDAMENTALS AND KNOWLEDGE RELEVANT TO THE DRAG REDUCTION THROUGH AIR CAVITATION OF SHIP'S HULLS

(Reference No: IJME693, DOI No: 10.5750/ijme.v163iA3.804)

E Amromin, Mechmath Limited Liability Company, USA

KEY DATES: Submitted: 29/12/20; Final acceptance: 25/05/21; Published 16/11/21

SUMMARY

Numerous experiments with ship drag reduction by air bottom cavitation in diverse countries have exhibited very different achievements. Therefore, a paper clarifying mechanics of this drag reduction and describing the proven design algorithms is appropriate. Solutions of an ideal fluid problem existing in diverse ranges of Froude number are compared and the solutions suitable for ship drag reduction are considered in more detail. It is emphasized in this paper that a cavity locker at the trailing edge of the bottom niche (recess) assigned for the cavity is necessary to reduce the necessary air supply to the cavity and to mitigate the cavity tail pulsation resulting in a drag penalty. It is also pointed out that the bottom niche depth must allow for cavity withstanding under impact of waves in seaways. Bottom cavitation may even reduce wave-induced loads on the hull. With taking into account the above-mentioned design aspects, the energy spent on the air supply can be minimized. An algorithm of bottom design based on ideal fluid theory is also explained in the paper. Comparisons with several model test results are provided to illustrate the algorithm employment.

NOMENCLATURE

C	Hydrofoil chord (m)
C_D	Drag coefficient
Cp	Pressure coefficient
Fn	Froude number
g	Gravity acceleration (m/s^2)
h	Distance from intermediate to corrected cavity surfaces (m)
LWL	Ship length (m)
l_C	Cavity length (m)
N	Normal to S
P_0	Ambient pressure (Pa)
P_C	Pressure in cavity (Pa)
q	Air supply (m^3/s)
Q	Dimensionless source intensity
Re	Reynolds number
S	Surface of careen and cavity (m^2)
V	Speed of ship (m/s)
U	Dimensionless water velocity
ρ	Density of water (kg/m^3)
Φ	Velocity potential (m^2/s)
Ψ_0	Ship trim (degree)
σ	Cavitation number
Δ	Laplacian operator

1. INTRODUCTION

Friction of a body moving in air is negligible in comparison with its friction in water at the same speed of motion. This fact was the origin of the idea of ship drag reduction by separation of a part of her hull by an air layer. This idea was first stated by Laval in his 1883 patent. Diverse devices for a practical realization of this idea were claimed in many patents quite soon. In USA, the first of them was submitted by Owen in 1885. However, the first successful application of ship bottom ventilation by air was reported by Basin et al (1969) only 86 years later (for a river ship). Planing boats of various displacements became commercially available a quarter of century ago. The following successes in application of this drag reduction technology to various full-scale ships (especially, for planning boats) were described by Butuzov et al (1990), Matveev et al (2009), Sverchkov (2010), Gorbachev and Amromin (2012), Dern et al (2015).

The broad experimental study of ship bottom ventilated cavitation with the corresponding attempts of the model design started quite recently. Numerous tests meeting these requests have been carried out in China, Italy, Korea, Netherlands, Russia, Sweden, UK and USA. However, in these studies variations of the measured energy saving rates (of the ratios of energy saved due to drag reduction minus the energy spent on the air supply to the whole spent energy) are very significant in the tests at low or moderate Froude number $Fn=V(gLWL)^{-0.5}$ reported by Foeth (2007), Makihurgu et al (2010), Allenstrom and Leer-Andersen (2010), Amromin et al (2011), Zverkhovski et al (2014), Butterworth et al (2015), Park and Lee (2018), Hao and Yongpeng (2019). In particular, the energy consumption on the cavity maintenance was below 1.5% of the total energy necessary to tow the model in the towing tests of Amromin et al (2011), whereas the total drag reduction was up to 25% there. This consumption was 7% of the total energy spent in the towing tests of Park and Lee (2018), whereas their total drag reduction was 18% there. Also, the minimal air supply rates (normalized using the cavity surface area and the inflow speed) have varied from 0.015 in the tests of Amromin et al (2011) and 0.04 in the tests of Makihurju et al (2010) up to 0.29 in the tests Butterworth et al (2015). Meanwhile the excessive air supply leads to both the direct loss of energy and its indirect loss due to an increase of the hull form resistance because an additional air flux thickens the boundary layer over the stern.

So, for many decades from the first full-scale success, only several other full-scale ships were built (including 8 fast ships mentioned by Sverchkov (2010) and 2 river ships). The absence of a description of the employed design algorithm in the papers reporting the experiment successes may contribute to this situation (in the best case, the main employed equations were provided). The aims of this paper are to point out design requirements neglected in the less successful model tests and to describe the proven algorithm of bottom design (or retrofit) in more detail. Data of already reported experiments are used here.

2. FUNDAMENTALS OF DRAG REDUCTION BYCAVITATION

Nevertheless, it is useful to recall the principles used in the bottom design. For ship drag reduction by an air layer, it is necessary to keep it stable allowing for the quite low energy consumption on the air supply. However, there are three phenomena making this difficult. The first one is the air buoyancy. The air tends go up to the atmosphere. Though the buoyancy effect becomes smaller with an increase of the ship speed, it remains significant within its ranges usual for ships because this effect increases with their length. The second one is the air entrainment by the surrounding water flow. As manifested by Arndt et al (2009), this entrainment may by reduced down to zero for low Reynolds number (laminar boundary layers over the air layer), but it unavoidable for turbulent boundary layers inherent to ship flows. The third one is the general unsteadiness of air (gas) volumes in water. Their pulsations lead to an additional drag. Also, these pulsations substantially increase the air escape (and consequently the air demand necessary to maintain such a volume).

There are, however, situations with the possibility to suppress such pulsations. Such a possibility was discovered by Butuzov (1966) more than a half century ago via a theoretical analysis. As one can find in Birkhoff (1971) review, the ideal fluid theory was the only model employed in theory of cavitating flows at that time. The general formulation of the corresponding problem includes Laplace equation for velocity potential

$$\Delta\Phi=0 \tag{1}$$

that is indeed the water mass conservation law among with the non-permeability condition for the flow boundaries S

$$\partial\Phi/\partial N|_S=0, \tag{2}$$

the pressure constancy condition for the cavity surface S^*

$$U^2+2P_c/\rho+2g(z-z_\infty)|_{S^*}=V^2+2P_\infty/\rho \tag{3}$$

and the condition of uniform incoming flow

$$grad(\Phi)|_{|x|\to\infty}=V \tag{4}$$

Here S^* is a part of S.

The problem (1)-(4) is nonlinear because there are two conditions on the same boundary. As a result, the boundary shape must be fitted to satisfy both of them and Eqs.(2) and (3) become nonlinear on S^* because the components of N are also initially unknown there. Generally, such problems require sophisticated methods of solving (like used by Amromin et al (2011) in particular). However, for 2D cavities under a flat wall (considered as a simplified shape of the ship bottom), Butuzov reduced this problem to a 2D problem distributing sources along the wall and derived a linear integral equation for the coordinate of cavity surface z

$$\frac{z}{Fn^2}-\frac{1}{\pi}\int_0^{l_c}\frac{dz}{d\tau}\frac{d\tau}{(\tau-x)}+\frac{\sigma}{2}=\left.\frac{dz}{dx}\right|_{x=0} ln\left|\frac{x}{a+x}\right|-\left.\frac{dz}{dx}\right|_{x=l_c} ln\left|\frac{l_c-x}{l_c-x+b}\right| \tag{5}$$

from linearized 2D equations (1)-(4). Here a is the cavitator length, b is length of the fictitious body (described by Knapp et al (1970) or in other monographs on cavitation) used for cavity closure when the time-average ideal fluid flows are analysed. There is a direct proportionality of b and cavitation-induced drag.

Figure 1: Solutions of Eq.(5) for cavities under flat wall

As one may see in Figure1, this equation has four types of solutions. Solutions of the type 1 can exist for unlimitedly high Fn. A larger cavity displaces water from a greater surface area and this may seem to be better for a greater friction reduction, but, as discovered by Butuzov, there is an upper Fn-dependent limit L_{max} of the cavity length l_C.

The problem solution for $l_C=L_{max}$ is the penalty-free cavity of type 2. The fictitious body behind such a cavity disappears. Linear theory gave an estimate $L_{max}\sim\pi V^2/g$ for the solutions of type 2 (the proportionality to the half-wavelength in linear wave theory).

Further, there is a range of smaller Fn, where the mathematical solution of the type 3 intersects the wall. As noted by Butuzov and later illustrated by photos made by Arndt et al (2009) and presented in Figure 2, there is no a stable cavity in the experiments within this range of Fn. In the above-mentioned experiments in particular, no stable cavity was observed for $0.31<Fn<0.43$.

Finally, at smaller Fn the solutions of type 4 with cavities of unlimited modulated by waves was found by Butuzov (1966). In the experiments of Arndt et al (2009) the wavy cavity was observed for $Fn<0.31$.

As reported by Butuzov et al (1990) and later recalled by Gorbachev and Amromin (2012), the solutions of types 2 and 4 (with similar cavities of limited lengths) were employed in design of built full-scale vehicles.

However, as illustrated by Figure 3, unlikely to pressure over flat plate, pressure on bottoms of real ships is far from constant and nonlinear effects on the cavity shapes are expected.

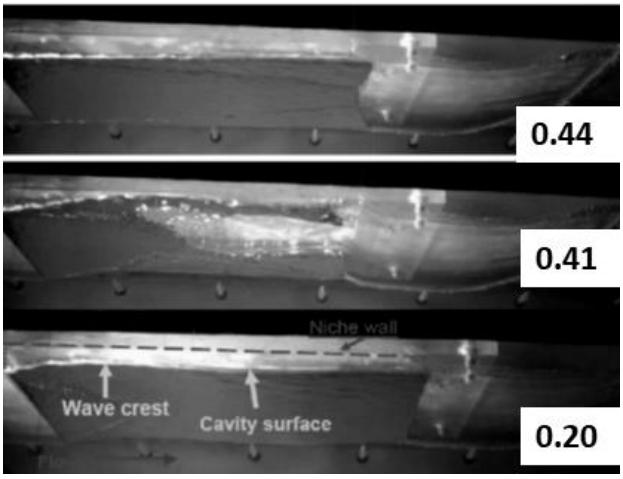

Figure 2: Observed cavities of the type 2 (*Fn*=0.44), type 3 (*Fn*=0.41) and type 4 (*Fn*=0.2) in a niche

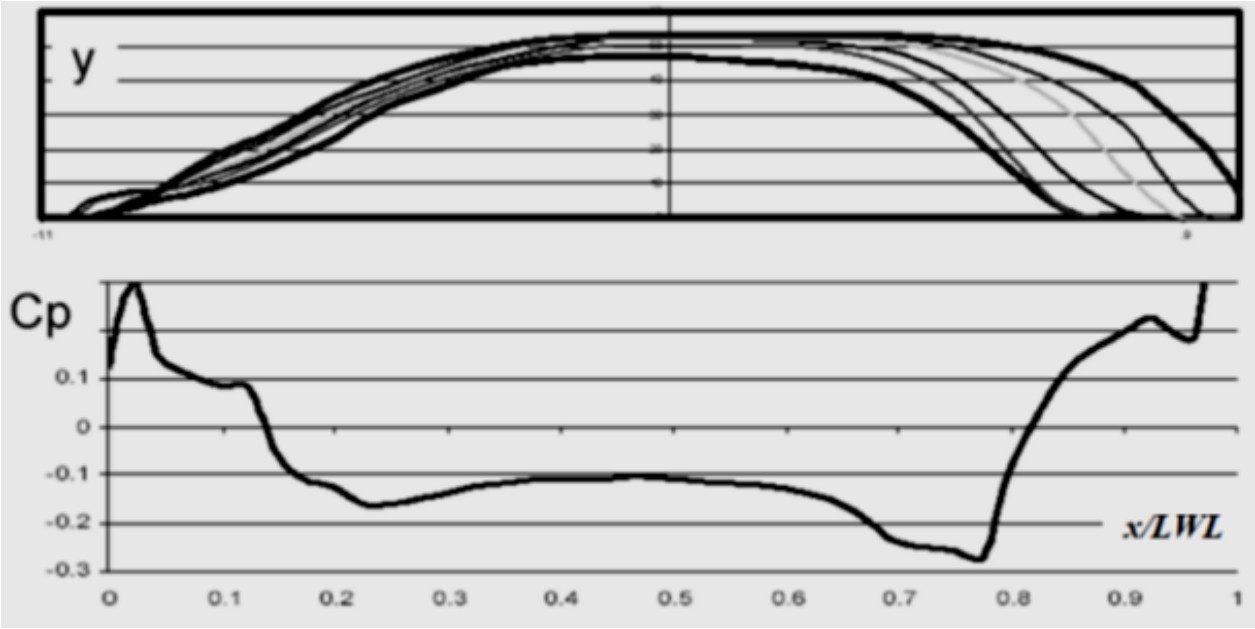

Figure 3: Lines plan of the TAO-187 hull with the flat bottom (up) and variation of dimensionless pressure coefficient *Cp* along its vertical symmetry plane at very small *Fn* (down)

Some further design attempts were based on nonlinear solutions of Eqs.(1)-(4). First validation of the elaborated nonlinear design algorithm was carried out by Amromin et al (2006) for the hydrofoil because the water tunnel experiments are cheaper and better observable.

Like the design of river ships described by Butuzov et al (1990), design of such a hydrofoil was basically a retrofit of some existing shape. The existing shape selected by Amromin et al (2003) was hydrofoil NACA0015. As shown in the upper part of Figure 4, shape of the partial cavity of the length l_C=0.6C computed for 5 degree angle of attack with a parabolic fictitious body was employed in design of a new hydrofoil named as OK2003; its coordinates were published by Amromin and Arndt (2019).

Comparison of pressure distributions for both hydrofoils in cavitation-free conditions is provided in the lower part Figure 4. As seen in the upper part of this figure, the fictitious contour for cavitating NACA0015 plays the role of a cavity locker for designed OK2003.

As seen in Figure5 with the results of water tunnel tests, the design of OK2003 makes it possible a significant drag reduction by cavitation in quite wide ranges of cavitation number $\sigma = 2(P_0-P_C)/(\rho V^2)$ and angles of attack. Such a possibility appeared due the substantial pressure minima just downstream of the cavity and was associated with suppression of the cavity tail oscillation (of re-entrant jets) within these ranges. As also seen in Figure 5, at much smaller cavitation number larger cavities cut such minima and the corresponding C_D goes to the values usual for supercavitation.

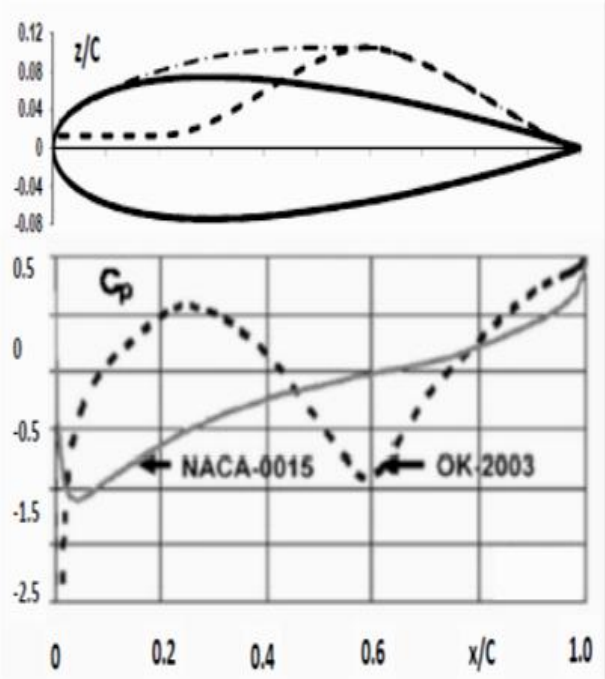

Figure 4: Shapes of hydrofoils OK2003 and NACA0015 (in the top; the cavity section is shown by dashed –dotted line, contour of NACA0015-by solid line, the pressure side of OK2003 coincides with the pressure side of NACA0015, the suction side of OK2003 shown by dashed line; the common part of dashed and dashed-dotted lines is the fictitious contour for cavitating hydrofoil NACA0015) and pressure on the suction sides of hydrofoils in cavitation – free flows (in the bottom).

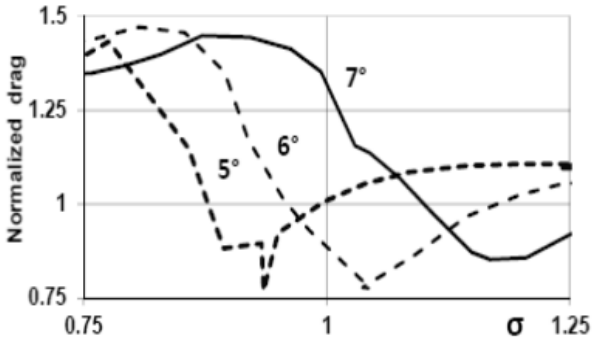

Figure 5: Measured drag of hydrofoil OK2003 at various angles of attack and cavitation numbers; C=0.08m

The water tunnel tests also manifested similar drag reduction rates for natural and ventilated cavitation. However, these tests in Saint Anthony Falls Laboratory (SAFL) were carried out at $Re<10^6$ and $Fn>11$. The Re values inherent to ships are much higher and their Fr values are much lower. Later the experiments Makihurju et al (2010) in W.B. Morgan Large Cavitation Channel (LCC) were carried out with a huge hydrofoil (C=12.9m). There was no possibility to measure hydrodynamic loads on it. However, this experiment allowed for observation of ventilated bottom cavities at Fn values inherent to some ships. Also, the values of Re were much closer to values inherent to real ships. The tests were carried out with the same cavitator (hydrofoil leading part) and with a half of dozen different lockers (one of them is shown in Figure 6 among with cavity shapes computed using the method employed in design of OK2003).

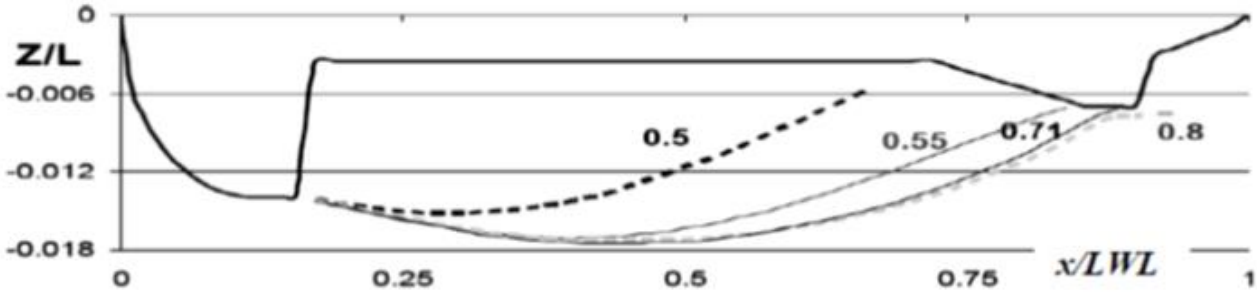

Figure 6: Computed cavity shapes for the model tested in LCC. Solid line is buttock. Numbers at lines show Fn values.

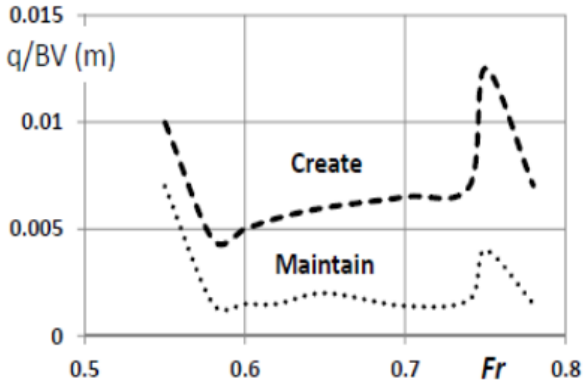

Figure 7: Air demand of the model tested in LCC for the cavity creation and maintenance

As seen in Figure 7, for the best locker a small air demand was sufficient to both create and maintain cavities between Fn=0.57 and Fn=0.73. It was found in LCC tests that a 30% variation of the heigth of the locker increases the air demand more than twofold. As one can conclude from the computed cavity shapes plotted in Figure 6, the best locker allows for cavity shapes of the type 2 at least within the range $0.55 \le Fn \le 0.71$. It is also important to note that the cavity shape at Fn=0.55 is close to its shape at Fn=0.71, whereas at Fn=0.5 and Fn=0.55 they are not.

So, the shapes of ventilated cavities can be satisfactory predicted using ideal fluid theory (at least for steady inflows). The cavity contents insignificantly affect these shapes (as shown by Amromin and Arndt (2019) in

particular). The bottom boundary layer has not a significant impact on them, as one can understand also from the later special experiments of Barbaca et al (2019).

3. DESIGN ALGORITHM FOR BOTTOM ADJUSTMENT TO VENTILATION

One can see in Figure4 that the contour of OK2003 was designed on the basis of solution of the problem with Eqs. (1)-(4) for the hydrofoil NACA0015 with a partial cavity and some fictitious body downstream of it, but no unique algorithm for transformation of the surface *S* from this solution to the above-mentioned contour was described yet. Meanwhile, capability of drag reduction within a range of *Fn* depends on such an algorithm. Moreover, it is necessary to point out that the employed algorithm of the locker design (hull retrofit) to drag reduction by air cavitation is based on solving nonlinear problem with Eqs.(1)-(4) because 2D linear equation (5) derived for the flows under flat walls was sufficient only for comprehension of fundamentals of drag reduction, but it is insufficient for a practical design. Practically it is necessary to design a locker for a range of *Fn*, but even its design for a single *Fn* value is the nonlinear problem and the corresponding design procedure is based on an iterative procedure involving equations that are more complex than Eq.(5) is.

Any iteration consists of two steps. First, the distribution of U=|grad(Φ)| over the hull and over the cavity of its intermediate shape is computed using Eqs.(1),(2),(4). These 3D computations for a ship can be carried out using BEM or RANS solvers. Second, if Eq.(3) is not satisfied by the obtained U with the required accuracy, the shapes of cavity and its locker (fictitious body) must be corrected (otherwise that shape will be considered as the solution).

Because the flow in the niche slightly depend on the lateral coordinate, this correction can be based on solving several equations

$$Q\{x\} = \frac{R\{x\}}{\pi}\int_0^{l_c}\frac{\left[U^2-1-\sigma+2(z+N_z)Fn^2\right]}{U(x-\tau)R\{\tau\}}d\tau \quad (6)$$

for several sections y=const. Here the abscissas are counted from the leading edge of the niche, and the cavity length for each value of y must be found from the condition

$$\int_0^{l_c}\frac{\left[U^2-1-\sigma+2(z+N_z)Fn^2\right]}{UR\{\tau\}}d\tau = 0 \quad (7)$$

and $R\{x\} = \sqrt{x(l_c - x)}$. Then the necessary corrections for each y=const can be determined after solving equations (6) and (7) via the formula

$$h\{x\} = \frac{\beta}{2U}\int_0^x Q\{\tau\}d\tau \ , \quad (8)$$

where the factor $0.2<\beta<0.4$ is introduced for the better convergence of iterations. One can find the multi-step derivation of linear two-dimensional equations (6)-(8) from the original three-dimensional nonlinear system of equations (1)-(4) in the paper of Amromin (2007).

Additional explanation for design of a locker assigned to drag reduction within a range of speed is provided in the legend to Figure8. This illustration relates to the ship model 5694 described by Amromin et al (2011) and tested in the Linear Towing Tank of David Taylor Model Basin.

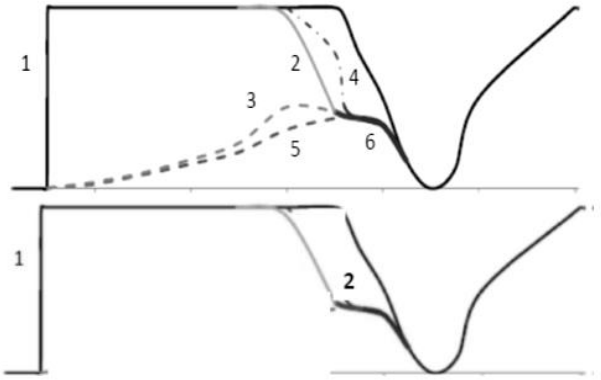

Figure 8: Scheme of a locker design. Upper plot: Succession of design steps. Line 1 is an initial buttock. Line 5 is the section of cavity corresponding to Fn_1, line 6 is the section of its fictitious body, line 4 shows the locker intermediate shape, line 3 is the section of cavity corresponding to Fn_2, a short thick solid line between lines 3 and 6 is the section of its fictitious body. The locker section starts as the line 2 (that is a curve smoothly connected to both Line 1 and Line3). Further it includes the line 6 and finally joints to the initial wall of the niche (the rear part of the line 1). Lower plot: Initial (Line 1) and final (Line 2) niche sections.

The design procedure for the range $Fn_1<Fn<Fn_2$ is based on two subsequent designs for the range edges. Its illustration in Figure 8 is provided without an account of the trim effect on the flow around the ship. However, for $Fn>0.4$ the ship trim significantly influences the pressure over the hull.

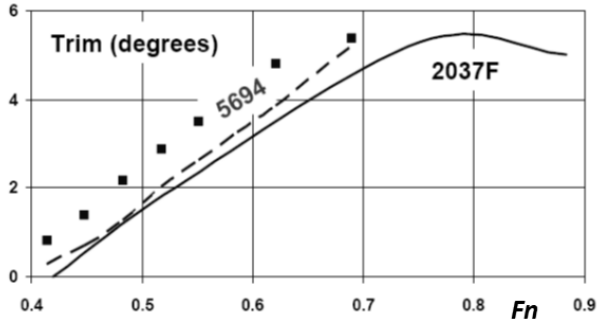

Figure 9: Trim of three towed models versus *Fr*; solid line – for Davidson Laboratory planing model 2037; rhombus – for model 5694 with cavity, dashed line –for baseline model 5694 without any niche for cavity.

As shown in Figure 9 with comparison of experimental data of Davidson Laboratory (1966) and Amromin et al

(2011), the dependencies $\Psi_0(Fn)$ are similar (and even close) for diverse ship. Moreover, the bottom cavity insignificantly changes these dependencies.

On the other hand, as one can conclude comparing the cavity in Figure10 with the cavities in Figure 8 for the same bottom, the trim substantially affect the cavity shapes. This circumstance must be taken into account in the design algorithm. Therefore for such Froude numbers the problem (1)-(4) must be solved for two edges of the considered interval of *Fn* at two different Ψ_0. The values of Ψ_0 for the baseline hull without cavity and for the designed hull are quite close.

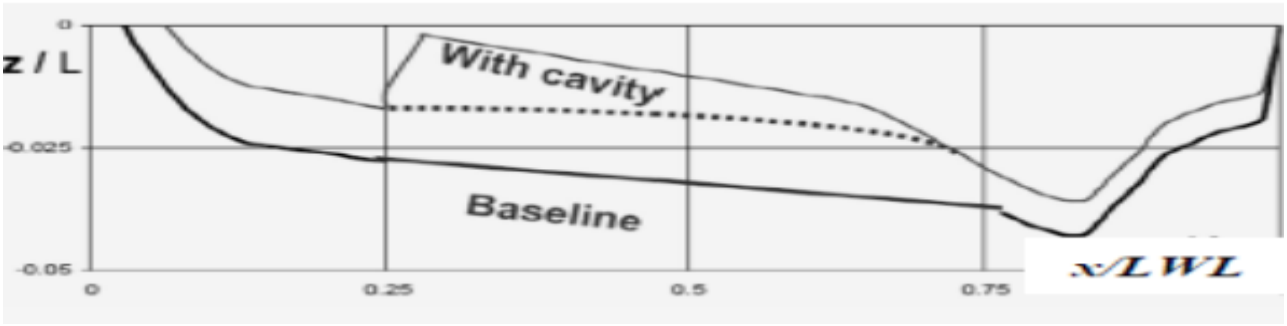

Figure 10: Submerged parts of the buttocks at *Fn*=0.48. Computations were made for the same displacement.

The bottom of model 5694 is shown in Figure 11. The hull form is different from a traditional form (like shown in Figure 3) because this model was planned to be the unit of a cross-ocean seatrain (one can find more detail on seatrain project in the paper of Mizine and Karafiath (2015) in particular). The model bow and stern was adjusted just to such a goal.

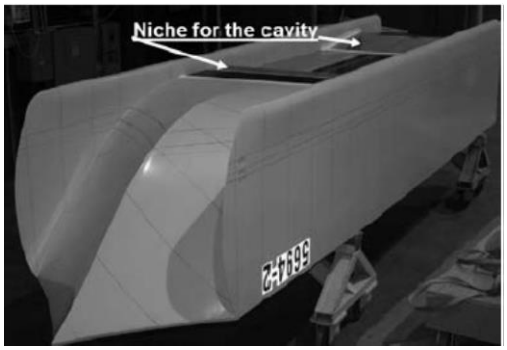

Figure 11: Bottom view of the model 5694 tested in David Taylor Model Basin

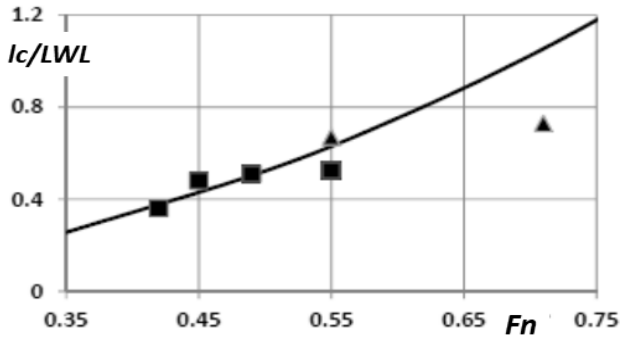

Figure 12: Dependencies of cavity length on Froude number. Line is the dependency $l_C=\pi Fn^2 LWL/5$, triangles relate to model tested in LCC, squares – for model 5694

Cavitation number for the model 5494 with cavity varied from σ=-0.28 at *Fn*=0.45 to σ=-0.13 at *Fn*=0.55. The values of σ are negative due to ventilation by air under excessive pressure. As seen in Figure 12, there is not the direct proportionality of l_C to Fn^2 for the cavities in the niches, though linear theory may give an estimate to their minimal stable length.

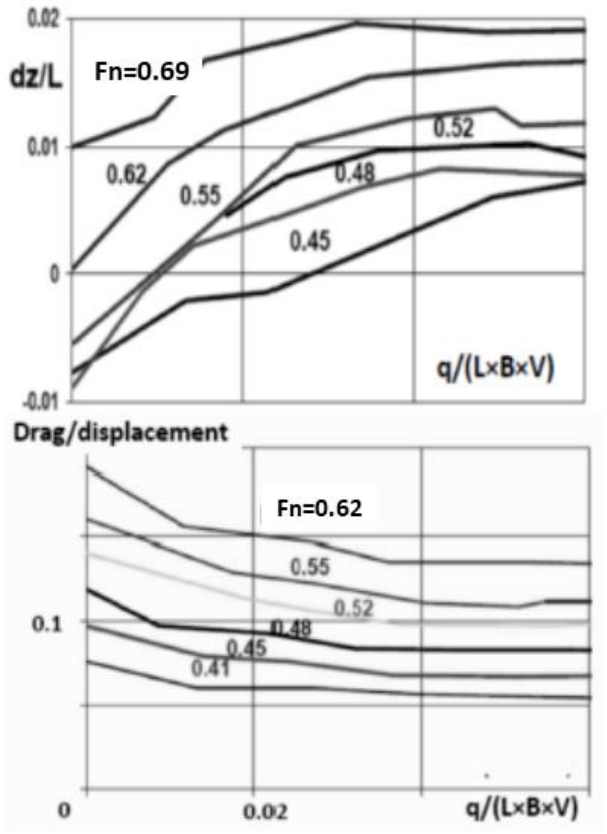

Figure 13: Influence of air supply rate on heavy dz of the towed model 5694 (in the top) and on its drag to displacement rate (in the bottom); B is model beam

The effects of augmentation of air supply rate are illustrated by Figure 13. As seen in the upper part of this

figure, this augmentation provides the additional buoyancy to the hull increasing its elevation from water and reducing the wetted surface area on the hull sides. However, this trend takes place only below some threshold values of *q*. As seen in the lower part of the same picture, the drag reduction rates achieved their maxima practically at the same values of *q*.

So, as pointed out by Amromin et al (2011), reduction of viscous drag is not directly proportional to the hull surface area covered by the cavity. Indeed there is a synergy of drag reduction effects.

4. EFFECTS OF THE NICHE DEPTH

For the model 5494 in particular this synergy was caused mainly by reduction of the wetted surface area shown in Figure 14. It is evident that this reduction is coupled with the cavity volume and, consequently, with the niche depth.

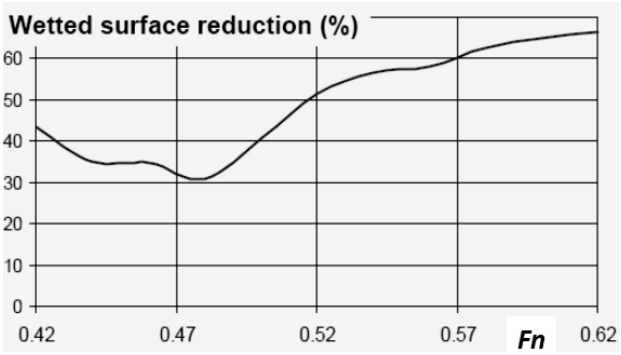

Figure 14: Variation of wetted surface area reduction with variation of *Fn* for model 5494

The niche depth is also important for mitigation of sea wave impact on ship motions. As shown in Figure 15, a wave impact increases drag of a ship with bottom cavity, but for the similar ship without such a cavity this increase is much higher. Figure 15 with the extrapolated results of model drag measurement in DTMB linear towing tank was plotted for a 90m length ship corresponding to the model 5494; the niche depth of such a ship would be 1.35m. One will see that a significant drag reduction can be kept for such a ship with the niche of this depth in Sea State 5.

Some drag reduction will be kept at higher sea states. However, even for the sea state 6 the cavity in the same niche would be periodically destroyed by waves and the air supply necessary for its periodical restoration (creation) would be too high and would not allow for an energy saving. Therefore, the cavity decay caused by interaction with the 10% probability wave could be assumed as a limiting event. Consequently, the magnitude of a 10% probability wave should be smaller than the niche depth.

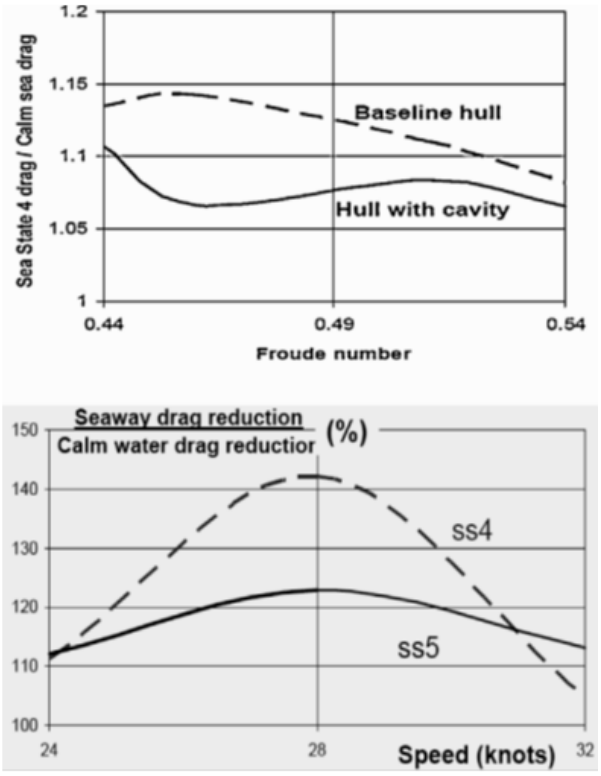

Figure 15: Measured wave impact on drag of ship model 5694 with cavity and on her baseline hull in towing tank with wave corresponding to sea state 4 for the 90m length ship (top) and percentage of drag reduction by cavitation kept in head sea states 4 and 5 by such ship of 90 m length (bottom).

Also, as pointed out in the book edited by Dern et al (2015), the bottom cavity can substantially reduce wave-induced vertical acceleration of the hull. So, the deeper niche improves the response of a ship with bottom cavity to the sea wave impact. On the other hand, the deeper niche affects the general ship arrangement and reduces her stability (the interior keels seen in Figure 16 are inserted to minimize this reduction).

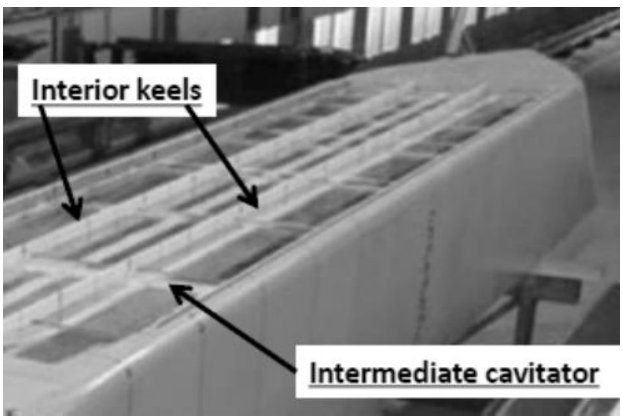

Figure 16: View of a model with the niche designed for the cavity of type 4

The bottom of the model shown in Figure 16 was designed for the cavity of type 4. For small *Fn* values inherent to

the majority of cargo ships such cavities could give a higher drag reduction rate. However, as illustrated by Figure 17 taken from Gorbachev and Amromin (2012) paper, this design is more sensitive to variations of trim leading to the cavity decay.

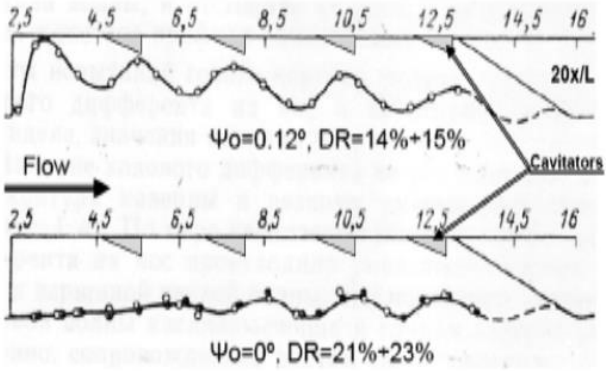

Figure 17: Effect of trim on cavity shape and drag reduction at *Fn*=0.14 for a tanker model

For the ship hull with such a design (like model of the fullness coefficient 0.872 tested by Gorbachev et al (2015) and assigned for *Fn*=0.16) a synergy of drag reduction effects is caused mainly by the reduction of boundary layer thickness on the hull stern. This reduction results in a decrease of form resistance and even in preventing of boundary layer separation on the stern.

In the long-term drag prognoses an additional advantage of bottom cavities is associated with biofouling that can substantially affect energy consumption by ships with traditional hulls, as described by Demirel et al (2017). Because, as already manifested by Amromin and Arndt (2019), inclusions in the cavities do not affect the drag biofouling within the niche will not affect this consumption. So, selection of the niche depth should by a compromise between several opportunities and restrictions. Various numerical methods capable to solve 3D problem (1)-(4) are well developed now.

5. REMARKS ON DESIGN VALIDATION

The described design algorithm works in the framework of ideal fluid theory. The nonlinear design problem was solved by the iterative method employed Eqs.(6)-(8), but there are also other methods to solve such problems (see the paper of Choi and Chahine (2010) for an example). However, ideal fluid theory cannot provide the actual drag values and drag reduction rates.

In the ship design practice model tests in towing tanks are the unavoidable steps. Nevertheless, a preliminary computational validation of design results would be highly desirable. The tools of this preliminary computational validation already achieved a high accuracy in drag predictions for cavitation-free ship hulls reported by Stern et al (2012). There are also satisfactory results of force computations for various 3D cavitating flows achieved with RANS and LES solvers. However, no well validated computational tools for drag estimation for ships with air bottom cavities were elaborated yet. Possibly, the existence of very intensive reverse velocities within ventilated cavities makes it difficult to fit the employed wall functions of the above-mentioned solvers to computation of flows with ventilated cavities (according to measurements of Yoon et all (2020), these velocities can be around -0.5*V* for cavities in niches,).

Because the bottom adjustment for cavity is not a trivial (and standard) procedure, it is reasonable to compare the ventilated cavitation achievements with the achievements of other proven technologies. Stern flaps gave up to 15% drag reduction for approximately two hundreds of US Navy ships at $0.35<Fn<0.65$, but no description of stern flaps application of this technology for commercial ships was found. Drag reduction by microbubbles technology looks simpler than drag reduction by air bottom cavitation. According to American Bureau of Shipping (2019), that technology suitable for relatively small *Fn* was already employed on twenty three ships. However, their achieved energy saving has been between 4% and 5% only. The proven energy savings for ships with bottom cavities (15% to 25%) were much better.

6. CONCLUSIONS

Drag reduction by cavitation can provide the greatest drag reduction rates among technologies proven for ships. The contribution of late Anatoly Butuzov (born in 1931) was decisive for the success of this technology. Successfully designed/retrofitted bottoms of ships with ventilated air cavities can substantially (up to 25%) reduce the energy consumption necessary for their motions. Meanwhile, numerous tests of ship models with drag reduction by air bottom cavitation in diverse countries have exhibited very different achievements. Such a difference should be explained.

The theoretical fundamentals of adjustment of ship bottom to drag reduction by cavitation are explained in this paper. It is pointed out that a cavity locker at the trailing edge of the bottom niche (recess) assigned for the cavity is necessary to reduce air supply to the cavity and to mitigate the cavity tail pulsation resulting in a drag penalty. The bottom cavitation may even reduce wave-induced loads on the hull.

An algorithm of bottom design based on ideal fluid theory is also explained in the paper. The main equations employed for determination of the locker shape are provided. Comparisons with several results of previously provided model tests are employed as validation examples for this algorithm.

7. REFERENCES

1. ALLENSTROM, B, LEER-ANDERSEN, M. (2010) *Model Tests with Air Lubrication*. International Conference on Ship Drag Reduction, Istanbul

2. AMERICAN BUREAU OF SHIPPING (2019) *Air Lubrication Technology*.(accessed on 23 May 2021) https://ww2.eagle.org/content/dam/eagle/advisories-and-ebriefs/AirLubricationTechnology.pdf
3. AMROMIN, E.L. (2007) *Design of bodies with drag reduction by partial cavitation as an inverse ill-posed problem for velocity potential.* 9th Conf. Numerical Naval Hydrodynamics. Ann-Arbor
4. AMROMIN, E.L., ARNDT, R.E.A (2019) *Analysis of influence of cavity content on flow pulsations.* International J, Multiphase Flows v110, pp108-117
5. AMROMIN, E.L., KARAFIATH, G., METCALF, B. (2011) *Ship drag reduction by air bottom cavitation in calm water and in waves*. J. Ship Res. v55, pp.196-207
6. AMROMIN, E.L., KOPRIVA, J., ARNDT, R.E.A., VOSNIK, M. (2006) *Hydrofoil drag reduction by partial cavitation*. ASME J. Fluids Eng. v128, pp.931-936
7. ARNDT, R.E.A., HAMBLETON, J., KAWAKAMI, E., AMROMIN, E.L. (2009) *Creation and maintenance of cavities under horizontal surfaces*. ASME J. Fluids Engineering v131, p.111301
8. BARBACA, L., PEARCE, B.W., BRANDNER, P.A. (2019) *An experimental study of cavity flow over a 2-D wall-mounted fence in a variable boundary layer***.** International J**.** Multiphase Flows v105, pp.234-249
9. BASIN, A., BUTUZOV, A., IVANOV, A., OLENIN, Y., PETROV, V., POTAPOV, O., RATNER, E., STAROBINSKY, V. and ELLER, A. (1969) *Operational tests of a cargo ship 'XV VLKSM Congress' with air injection under a bottom*. River Transport, pp.52-53 (in Russian)
10. BIRKHOFF, G. (1971) *Mathematical Analysis of Cavitation*. UITAM Symposium on High-Speed Water Flows, Leningrad
11. BUTTERWORTH, J., ATLAR, M., SHI, W. (2015) *Experimental analysis of an air cavity concept applied on a ship hull to improve the hull resistance*, Ocean Eng. v110, pp.2–12
12. BUTUZOV, A.A. (1966) *Limiting parameters of an artificial cavity formed on the lower surface of a horizontal wall.* Fluids Dynamics v2, pp.116-118
13. BUTUZOV, A.A., GORBACHEV, Y.N., IVANOV, A.N, KALUZHNY, V.G., PAVLENKO, A.N. (1990) *Ship drag reduction by artificial gas cavities*. Sudostroenie #11,pp. 3-6 (in Russian)
14. CHOI, J-K., CHAHINE, G.L. (2010) *Numerical Study on the Behaviour of Air Layers Used for Drag Reduction.* 28th Symposium on. Naval Hydrodynamics, Pasadena
15. DAVIDSON LABORATORY (1966) *Reports on hydrodynamic model tests of high speed wheeled amphibian concepts.* Report 726-11. Hoboken
16. DEMIREL, Y.K., TURAN, O., INCECIK, A. (2017) *Predicting the effect of biofouling on ship resistance using CFD*. Applied Ocean Res. v62, pp.100–118
17. DERN, J-C., QUENEZ, J-M., WILLSON, P. (editors) (2015) *Compendium of ship hydrodynamics*, ENSTA, Paris, 638p
18. FOETH, E.J. (2008) *Decreasing frictional resistance by air lubrication.* 20th International Hiswa Symposium on Yacht Design and Yacht Construction, Amsterdam
19. GORBACHEV, Y.N., AMROMIN, E.L. (2012) *Ship drag reduction by ventilation from Laval to near future: Challenges and successes*. Conference of Association Technique Maritime et Aeronautique, Paris
20. GORBACHEV, Y.N., SVERCHKOV, A.V., GALUSHINA, M.V. (2015) *Propulsion of displacement ships with the single bottom cavities.* Sudostroenie #1, pp.17–23 (in Russian)
21. HAO, W.U., YONGPENG, O.U. (2019) *Numerical simulation of air layer morphology on flat bottom plate with air cavity and evaluation of the drag reduction effect*. International. J. Nav. Arch. Ocean Eng. *v*11, pp.210-220
22. KNAPP, R.T., DAILY, J.W. and HAMMIT, F.G. (1970) *Cavitation*, McGraw-Hill, New York, 578p.
23. MAKIHURJU, S., ELBING, B. R., WIGGING, A. DOWLING, D. R. PERLIN, M. and CECCIO, S. L. (2010) *Perturbed Partial Cavity Drag Reduction at High Reynolds Numbers.* 28th Symposium on. Naval Hydrodynamics, Pasadena
24. MATVEEV, K.I., BUMETT, T.J., OCKFEN, A. E. (2009) *Study of air-ventilated cavity under model hull on water surface*. Ocean Eng. v36, pp.930-940
25. MIZINE, I., KARAFIATH, G. (2015) *Model Test Evaluation of High Speed Trimaran (HST) Sea Train Concept.* 13th International Conference on Fast Sea Transportation, Washington
26. PARK, S.H., LEE, I. (2018) *Optimization of drag reduction effect of air lubrication for a tanker model*. International J. Nav. Arch. Ocean Eng. v10, pp.427-438
27. STERN, F., YANG, J., WANG, Z., SADAT-HOSSEINI, H., MOUSAVIRAAD, M., BHUSHAN, S. and XING, T. (2012) *Computational Ship Hydrodynamics: Nowadays and Way Forward*, 29th Symposium on Naval Hydrodynamics, Gothenburg
28. SVERCHKOV, A.V. (2010) *Application of Air Cavities on High-Speed Ships in Russia*. International Conference on Ship Drag Reduction, Istanbul

29. YOON, K., QIN, S., SHAO, S., HONG, J. (2020) *Internal flows of ventilated partial cavitation*, Experiments in Fluids v61, p.100
30. ZVERKHOVSKYI, O., VAN TERWISGA, T., GUNSING, M., WESTERWEEL, J. and DELFOS, R. (2014) *Experimental Study on Drag Reduction by Air Cavities on a Ship Model*, 30th Symposium on Naval Hydrodynamics, Hobart

